

---

# A Simple and Generalist Approach for Panoptic Segmentation

---

Nedyalko Prisadnikov<sup>1</sup> Wouter Van Gansbeke<sup>\*</sup> Danda Pani Paudel<sup>1</sup> Luc Van Gool<sup>1</sup>

## Abstract

Panoptic segmentation is an important computer vision task, where the current *state-of-the-art* solutions require specialized components to perform well. We propose a simple generalist framework based on a deep encoder - shallow decoder architecture with per-pixel prediction. Essentially fine-tuning a massively pretrained image model with minimal additional components. Naively this method does not yield good results. We show that this is due to imbalance during training and propose a novel method for reducing it - centroid regression *in the space of spectral positional embeddings*. Our method achieves panoptic quality (PQ) of **55.1** on the challenging MS-COCO dataset, *state-of-the-art* performance among generalist methods.

## 1. Introduction

Panoptic segmentation (Kirillov et al., 2019) is a dense prediction computer vision task that combines semantic and instance segmentation. It consists of labeling each pixel of an input image with its corresponding semantic category, as well as the specific instance to which it belongs. It tackles both *stuff-like* instance-less categories (like sky, grass, etc) and *thing-like* categories with potentially multiple instances per image (people, cars, etc). Solving segmentation tasks is useful for numerous real world applications including autonomous driving (Cordts et al., 2016; Mohan & Valada, 2021), agriculture (Darbyshire et al., 2023; Chiu et al., 2020), medical imaging (Zhang et al., 2018; Menze et al., 2014), etc.

The instance segmentation part of the task requires solutions to be permutation invariant. Swapping the labels between two instances of the same class is still a valid solution. This poses a significant challenge. Earlier solutions required specialized components like region proposal networks (He

et al., 2017; Vasconcelos & Cai, 2017). Recent *state-of-the-art* approaches (Jain et al., 2023; Li et al., 2023; Cheng et al., 2021; Yu et al., 2022) propose an end-to-end strategy by casting the problem as a direct set prediction task. They achieve strong results but require a complex loss function based on bipartite matching, and contain transformer decoders with object queries (Carion et al., 2020), specialized for segmentation and detection tasks.

The vision community vouch for the use of generalist architectures (Lu et al., 2022; 2024; Wang et al., 2023) that can lead to models generalizing across multiple tasks. We propose a very simple deep encoder - shallow decoder framework with per-pixel prediction for the panoptic segmentation task. Using a strong pretrained image model (DINOv2 (Oquab et al., 2023)) as an encoder, and adding minimal architectural components to make it suitable for dense tasks. Namely, a shallow decoder that upscales the patch level representations to pixel level ones. Using a per-pixel prediction with averaged pixel loss makes it easy to apply this framework to different dense tasks.

This approach has worked well for some problems, but lags behind for panoptic segmentation. We will show that naively applying this framework for panoptic segmentation suffers from inherent imbalance during training. Understanding the source of it, we propose simple solutions that enable us to bridge the gap between generalist and specialized methods. Our main contributions are the following.

- We bridge the gap between specialized and generalist models using a simple method that can be described as fine-tuning DINO, while also performing well in a multi-tasking setup.
- We propose a novel approach (Section 3.3.1) for reducing the imbalance between small and large objects while training instance segmentation through centroid regression.

With per-pixel prediction, the permutation invariance of the instance labels can be addressed with deterministic labeling. We follow (Kendall et al., 2018; Cheng et al., 2020; Wang et al., 2023) and cast the instance segmentation problem as a pixel regression one. For each pixel we predict the location of the center of mass of the instance it belongs to.

<sup>1</sup>INSAIT, Sofia University "St. Kliment Ohridski". Correspondence to: Nedyalko Prisadnikov <first.last@insait.ai>. <sup>\*</sup>Supervised the first author while at INSAIT, now affiliated with Google DeepMind.

We show that performing direct centroid regression on the pixel level is prone to significant imbalance while training. By making a prediction of the spectral sine-cosine positional embeddings of the centroid coordinates instead (Section 3.3.1), we lift them to a higher-dimensional space where the imbalance is reduced. We give a detailed rationale behind this approach (Section 4), backed by strong experimental evidence (Section 5).

Additionally, we use a boundary aware loss modulation (Zhen et al., 2019; Zhang et al., 2019; Šarić et al., 2023; Zhu et al., 2019) in the form of edge distance sampling (EDS). This helps us to focus on *harder* pixels. We further show that EDS helps minimize the training imbalance between small and large objects.

With these we set a new *state-of-the-art* performance for panoptic segmentation among generalist methods. We achieve panoptic quality of **55.1** on MS-COCO (Lin et al., 2014).

## 2. Related work

**Panoptic segmentation** is one of the more challenging segmentation tasks. Semantic segmentation can be solved by simply classifying each pixel independently. With instance segmentation such a simple approach is not directly applicable. On top of classifying each pixel, we need to cluster pixels belonging to the same instance in a permutation invariant way. This challenge has forced solutions to use custom components. *State-of-the-art* methods are based on DETR (Carion et al., 2020) - a transformer decoder with object queries. They cast the problem as direct set prediction. The model outputs a set of masks, then a bipartite matching is applied between the predicted and target masks using Hungarian matching (Kuhn, 1955). This works very well, but requires a complicated loss mechanism. Also, the majority of the model’s parameters and computational complexity lie in the transformer decoder, which is specialized for generating segmentation masks. With the appearance of strong ViT-based (Dosovitskiy et al., 2021) image representation models, we ask ourselves if it is possible to reuse these strong general representations with minimal additional architectural components.

**Denosing diffusion methods.** Recently (Chen et al., 2023) and (Van Gansbeke & De Brabandere, 2024) proposed using denosing diffusion for generating panoptic masks, as a generalist framework. During training, they generate the target masks using random instance IDs with noise on top of them. The model learns to predict that specific random assignment of the label IDs. During inference the model is given random input noise and generates random assignment of the instance labels. This prevents the necessity of bipartite matching in the training loop. However, it

requires multiple denosing iterations to perform well.

**Methods with pixel-wise prediction.** If we want to use per-pixel prediction for panoptic or instance segmentation, we need a deterministic label for each instance. That way for each pixel we have a stable label to predict. A popular approach is using the coordinates of the center of mass of the instance as a label proxy (Kendall et al., 2018; Cheng et al., 2020; Wang et al., 2023). We base our work on this idea. Centroid regression has been used for panoptic segmentation in (Wang et al., 2023), but the gap to the *state-of-the-art* methods is significant. We will show simple modifications that unlock strong performance.

**Boundary aware per-pixel loss modulation** is a method used with pixel-wise loss to focus on the more challenging parts of the images (Zhen et al., 2019; Zhang et al., 2019; Šarić et al., 2023; Zhu et al., 2019), i.e. the pixels near object boundaries. We show that this approach also diminishes an imbalance between small and large objects during training. We perform Edge Distance Sampling (EDS) which only samples pixels near instance boundaries when computing the loss. The weight of each pixel is determined based on the distance to the nearest boundary.

## 3. Method

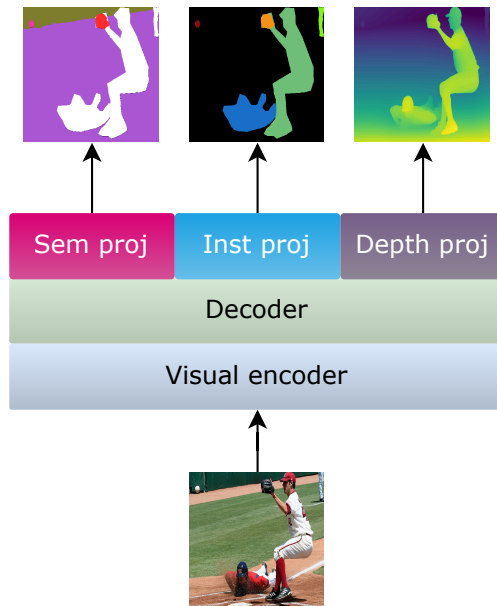


Figure 1. Overall model architecture in a multi-tasking setup. The vision encoder and the shallow decoder are shared among all tasks. The task specific projection heads are used only to map the decoded pixel embedding to the task required dimension. The depth prediction is an optional auxiliary task.

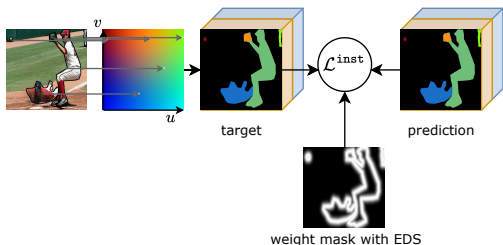


Figure 2. Schematic explanation of how labeling instances work. For each instance we find the  $u$  and  $v$  coordinates of its center of mass. Based on these coordinates we label each pixel belonging to the instance. The label is the concatenation of the positional embedding of the  $u$  and  $v$  coordinates, respectively. Hence the two colored third dimension of the target and prediction. Lastly, we apply a distance loss on this representation, but only for pixels near object boundaries according to EDS (Section 3.3.2).

### 3.1. Architecture and task setup

We present our work in a multi-tasking setup. The panoptic segmentation task is split into two separate tasks - semantic and class-agnostic instance segmentation. The outputs of the two are combined to produce panoptic predictions. We also add a third task to validate the generalist nature of our solution - monocular depth prediction. This task is optional, we report results with and without it.

We use a standard deep encoder - shallow decoder architecture, where both the encoder and the decoder are shared across the tasks. The encoder backbone is DINOv2 (Oquab et al., 2023), while the decoder consists of four transpose convolutional layers (Long et al., 2015). The main purpose of the decoder is to upscale the patch-level embeddings to pixel-level ones. In essence the majority of the parameters are in the foundation vision backbone, which we fine-tune. Finally, the output of the decoder is fed through a task specific projection layer, in order to produce output in the correct format for each task. See the overall architecture in Figure 1. Similar strategy, without the multi-tasking setup has already been applied with DINO - for example for semantic segmentation and depth (Yang et al., 2024a;b).

Let the input image be  $\mathbf{I} \in \mathbb{R}^{3 \times H \times W}$ . The output of the encoder is  $\mathbf{z} = f(\mathbf{I}) \in \mathbb{R}^{e \times H/p \times W/p}$ , where  $p$  is the patch size of the encoder transformer (Dosovitskiy et al., 2021) and  $e$  is the embedding dimension throughout the encoder. The output of the shared decoder is  $\mathbf{h} = g(\mathbf{z}) \in \mathbb{R}^{d \times H \times W}$ , where  $d$  is the embedding dimension used in the decoder. Then the task-specific projection layer maps the  $d$ -dimensional embedding into task specific output  $\hat{\mathbf{y}}^{\text{task}}$ .

### 3.2. Pixel-wise loss

Using task-specific projection layers, allows us to have a different number of output channels per task, and thus have freedom with the choice of the loss. With pixel-wise loss, we can use any task-specific loss as long as it is computed on the level of the pixels. The loss for each task  $\mathcal{L}^t$  is simply average of the loss across all pixels,

$$\mathcal{L}^t = \frac{\sum_{i=1}^H \sum_{j=1}^W w_{ij} L^t(\mathbf{y}_{ij}^t, \hat{\mathbf{y}}_{ij}^t)}{\sum_{i,j} w_{ij}}, \quad (1)$$

where  $t \in \{\text{sem}, \text{inst}, \text{depth}\}$ ,  $\mathbf{y}_{ij}$  is the  $(i, j)$  pixel in  $\mathbf{y}$ .  $L^t(\mathbf{y}_{ij}^t, \hat{\mathbf{y}}_{ij}^t)$  is the task loss for pixel  $(i, j)$ . Note that we perform weighted average using the weight coefficients  $w_{ij} \in [0, 1]$ . This is how we perform Edge distance sampling EDS (Section 3.3.2).

### 3.3. Panoptic segmentation

As already mentioned, we split panoptic segmentation into semantic and class-agnostic instance segmentation. They are solved independently with averaged per-pixel loss. Semantic segmentation is solved as a standard classification task with a cross-entropy loss. The output of the task specific head has  $N$  channels, where  $N$  is the number of categories in the dataset. The approach for instance segmentation is explained next.

#### 3.3.1. POSITIONAL EMBEDDINGS FOR CENTROID REGRESSION

We use the objects' centers of mass as a proxy for their instance segmentation labels. In other words, for each pixel we predict the centroid coordinates for the instance it belongs to. If a pixel does not belong to any labeled instance, we label it with a predefined *void* encoding. In this setup, the magnitude of the loss directly depends on the accuracy of the predicted centroid. Note, that the centroids are only meant as proxies for clustering the pixels into a set of instances. Beyond this, the accuracy of the predicted centroid is of no significance. However, high accuracy in the centroid prediction is required on the boundary between instances with close centers of mass. With distance based loss, the scale of the loss on the boundary between close-by instances can be low because their respective centers of mass are close-by. Even when the model is mistaken about which instance the pixel belongs to. This can lead to imbalance during training. A visual explanation of the source of this imbalance can be seen in Figure 3 accompanied with detailed explanation in Section 4.

To address this issue, we propose to not compute the loss as a distance in the 2D space of the centroid coordinates. Instead we predict the spectral positional embeddings of the centroid coordinates, and compute the loss in this higher-dimensional

space. There the distances between the embeddings of the centroids are more balanced. For example, two centroids that are close in the image space can be far in the space of the positional embeddings. Importantly for us, the scale of the loss for mistakes in different parts of the image becomes more equal.

Concretely, let  $u$  and  $v$  be the coordinates of the center of mass of a given instance. We first normalize them to be values in the range  $[-1, 1]$ . Then we apply positional embeddings as in (Vaswani et al., 2017; Mildenhall et al., 2021). The final representation of each pixel is given by the concatenation of the embeddings for  $u$  and  $v$

$$\mathbf{y}_{ij}^{\text{inst}} = \begin{cases} \text{concat}(\gamma(u), \gamma(v)), & (i, j) \in \mathbf{O}(u, v) \\ \mathbf{0} \in \mathbb{R}^{4L}, & (i, j) \text{ unlabeled,} \end{cases} \quad (2)$$

where pixel  $(i, j)$  either belongs to object  $\mathbf{O}(u, v)$  with centroid coordinates  $(u, v)$  or is unlabeled.

The positional embedding  $\gamma$  is defined as,

$$\gamma(p) = (\sin(2^l \pi p), \cos(2^l \pi p))_{l=0}^{L-1} \in \mathbb{R}^{2L}. \quad (3)$$

It is a  $2L$ -dimensional vector, where  $L$  is the number of harmonics we use. The output  $\hat{\mathbf{y}}^{\text{inst}}$  for the instance segmentation task is a  $4L$ -dimensional vector for each pixel.

The pixel loss for the instance segmentation task is computed as the average euclidean distance between the prediction and the target embeddings, of the  $u$  and  $v$  coordinates, respectively. It is

$$L^{\text{inst}}(\mathbf{y}_{ij}, \hat{\mathbf{y}}_{ij}) = \frac{1}{2} \left( \left\| (\mathbf{y}_{ij} - \hat{\mathbf{y}}_{ij})_{[1:2L]} \right\|_2 + \left\| (\mathbf{y}_{ij} - \hat{\mathbf{y}}_{ij})_{[2L+1:4L]} \right\|_2 \right). \quad (4)$$

During inference, the  $u$  and  $v$  coordinates are recovered from  $\hat{\mathbf{y}}_{ij}$  using the nearest neighbor search method, between the prediction and positions in a discretized  $uv$ -grid space. This discretization is used to make post-processing simpler.

### 3.3.2. EDGE DISTANCE SAMPLING

Although we compute a pixel-wise loss, we don't let all pixels contribute equally. We only train on pixels close to object boundaries. For each pixel  $(i, j)$  we compute the euclidean distance  $d_{ij}$  to the nearest boundary. Then the weight of that pixel is given by

$$w_{ij} = w_{\min} + (1 - w_{\min}) e^{-\frac{d_{ij}^2}{D^2}}. \quad (5)$$

Here  $w_{\min}$  is the minimum weight for pixels that are far away from boundaries. In our experiments  $w_{\min} = 0$ . The parameter  $D$  determines how quickly the weight decreases when going away from a boundary. We use a value of  $D = 20$  in our experiments. Example weight masks are shown in Figures 2 and 6.

Weight distribution in this manner helps us to focus on the image regions with highest information. It is akin to lateral inhibition in animal vision (Livingstone, 2022; Jernigan & McLean, 2018) which leads to higher activations only near edges. Similar approach is used in other works (Zhen et al., 2019; Zhang et al., 2019; Šarić et al., 2023; Zhu et al., 2019) with the goal of focusing the training on the more challenging areas of the image. Additionally, and more importantly to us, EDS addresses two key problems. First, it mostly discards unlabeled regions when computing the loss for instance segmentation. Second, it reduces the imbalance between small and large instances during training. Both are explained in detail in Section 4.

### 3.3.3. ADDITIONAL LOSSES.

We use two additional losses, total variation loss (Rudin et al., 1992) as a form of regularization and generalized DICE loss (Sudre et al., 2017; Crum et al., 2006). The DICE loss is used only for instance segmentation. Find more details about them in Appendix B.

## 3.4. Monocular depth prediction

We use depth to validate that our solution is generalist. Since our encoder-decoder framework with pixel-wise prediction is already suitable for depth, we do not have to add any new components or loss functions. Simply, we attach another projection layer to the shared decoder and apply the standard loss functions following (Yang et al., 2024a). Similarly to DepthAnything, we train in two stages - pre-training on relative depth with pseudo labels, and fine-tuning on metric depth with ground truth labels. The loss functions we use for depth are explained in greater detail in Appendix A. The pseudo labels used during pre-training come from DepthAnythingV2.

## 4. Rationale

In this section we explain the rationale behind our contributions, positional embedding based loss for the class-agnostic instance segmentation and Edge distance sampling (EDS). Despite being simple, they address important limitations of the proposed framework.

**Handling unlabeled regions.** Instance segmentation datasets contain unlabeled or *void* regions. This is either due to pixels belonging to stuff categories, or belonging to

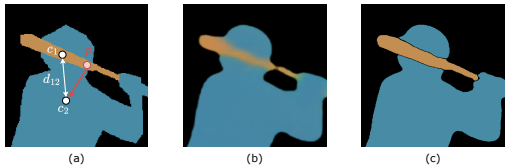


Figure 3. With centroid encoding of the instances, the scale of the loss for mistakes at the border between two instances depends on how far apart the two centroids are. Note, that here the distance  $d_{12}$  is not very small for visualization purposes, however, the model without PE based encoding (b) still struggles on the boundary. You can also see the prediction from a model trained with PE based encoding (c).

unlabeled objects. Because of the latter, these void regions should be ignored when computing the loss. However, with averaged pixel-wise loss, if we ignore the unlabeled regions, we fail to teach the model where objects end. This leads to a phenomena where the model’s predictions tend to expand instances, especially when they border an unlabeled region. See an example in Figure 6.

Solutions like Painter (Wang et al., 2023) treat the unlabeled void regions as background. This prevents the expansion issues, but wrongly penalizes the model when it predicts instances that are not labeled. When performing Edge Distance sampling (Section 3.3.2) with  $w_{min} = 0$ , we minimize the probability of such wrong penalization, while successfully preventing the expansion problem.

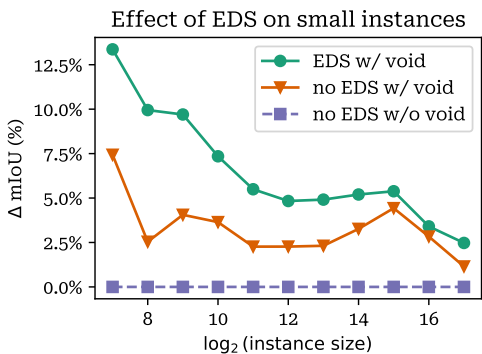


Figure 4. Effect of EDS on small instances. This charts shows that EDS has disproportionately bigger effect on smaller instances.

**Imbalance due to instance sizes.** Some of the most common problems when training with pixel-wise loss come from imbalance. Imbalance can be caused by categories which are under-represented in the data. But it can also be caused by some categories having instances of smaller size. An example consequence of such imbalance is when the

model’s loss is dominated by the small errors of already well predicted large objects, instead of by the large errors of poorly predicted small objects. This happens because large instances have much more pixels and thus overwhelm the averaged loss.

Edge distance sampling (Section 3.3.2) successfully reduces the imbalance due to object size. Intuitively, this is easy to understand with a simple example. Take two circles, the first one with radius  $R$ , and the second one with radius  $2R$ . The ratio of the areas of the two circles is 1 : 4. Hence, the second circle contributes 4 times more to the averaged loss. However, edge distance sampling mostly samples around the circumference of the two circles. Thus the contribution of the big circle will be roughly twice as large. Our experiments confirm this intuition. See the improvement caused by EDS plotted against object size in Figure 4.

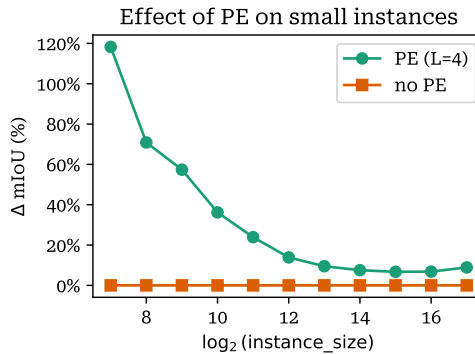


Figure 5. Effect of using PEs for the instance segmentation loss. The improvement of the Intersection-over-Union is much stronger for smaller objects.

**Imbalance due to difference in the scale of the loss.** Imbalance can also appear if the scale of the loss is different at different parts of the images. For the semantic segmentation task we use cross-entropy loss which is scale invariant. However, for the class agnostic instance segmentation through centroid regression, we use distance loss which is sensitive to the scale of the predicted values. Let us look at this through the example in Figure 3. With EDS we are only computing the loss near object boundaries. In Figure 3 point  $p$  is near the boundary of the instances with centers  $c_1$  and  $c_2$ . Let us say that the model wrongly assigns point  $p$  to the object with center  $c_2$ . Even then, the scale of the loss will depend on the distance between  $c_1$  and  $c_2$ . It is interesting to note that small neighboring instances are more likely to have their centroids close to each other. So small instances which already contribute to the loss with fewer pixels, now contribute even less because the scale of the loss is smaller than for large instances.

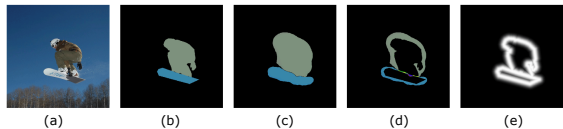


Figure 6. Instance expansion due to ignoring the void regions during training. The prediction (c) is much expanded compared to the target (b). The difference is shown in (d). A solution for this issue is the proposed Edge Distance Sampling (EDS). The weights obtained from EDS are shown in (e).

Using positional embeddings lifts the centroid coordinates to a high-dimensional space. In a way, we are using the curse of dimensionality (Bellman & Corporation, 1959; Bellman, 1961) in our favor. In a high-dimensional space the distances between sets of points are likely to be larger, leading to the contrast ratio of longest to shortest distance in a set of points being smaller. For example, consider an  $80 \times 80$  grid of  $uv$ -coordinates for the centroids. If we use L1 loss for direct regression of, say the  $u$  coordinate, then the ratio of the longest to shortest distance between any two points is approximately  $80 : 1$ . The distance to the furthest point is 80 times larger than the distance to the nearest neighbor. However, if we use PE based encoding with four harmonics ( $L = 4$ ), then the contrast ratio will be roughly  $5 : 1$ . This way the scale of the loss will be less dependent on how close the centroids are.

Another interesting observation here is the fact that the largest boundary in the COCO dataset is between an instance and a *void* region. So it is very important how we encode the void region and how "far" it is to other instances. If the encoding of the void region is far away from the instances, this opens a potential imbalance where the boundaries between an instance and the void region dominate the loss. We saw this empirically when training models without positional embeddings for the centroids. Boundaries between instances, especially if they are small, were much harder to learn, then boundaries between an instance and the *void* region. You can clearly see this in the second prediction of Figure 3.

## 5. Experiments

**Datasets.** We perform our experiments on three datasets. Panoptic segmentation on MS-COCO (Lin et al., 2014) and Cityscapes (Cordts et al., 2016), depth on NYUv2 (Silberman et al., 2012). MS-COCO consists of approximately 118K training and 5K validation images, with 80 thing classes and 53 stuff classes. Cityscapes consists of approximately 3K training and 500 validation high-resolution images. It contains 19 classes of which 8 are thing classes. For NYUv2 we use a 47K split for training and the official

Table 1. Panoptic segmentation results on COCO val2017 split. Our method achieves *state-of-the-art* results among generalist methods, while also performing well on depth.

METHOD	BACKBONE	PARAMS	PQ $\uparrow$
<i>Specialized methods:</i>			
MASKFORMER	SWIN-L	212M	52.7
MASK2FORMER	SWIN-L	216M	57.8
ONEFORMER	DINAT-L	223M	58
KMAX-DEEPLAB	CONVNEXT	232M	58.1
MASK-DINO	SWIN-L	223M	<b>59.4</b>
<i>Generalist methods:</i>			
UVIM	ViT-L	939M	45.8
PAINTER	ViT-L	303.5M	41.3
PAINTER-MT	ViT-L	303.5M	43.4
LDM-SEG	UNET	851M	43.3
PIX2SEQ-D	RESNET	94.5M	50.3
OURS W/ DEPTH	ViT-L	304.3M	<b>54.5</b>
OURS W/O DEPTH	ViT-L	304.3M	<b>55.1</b>

Table 2. Results for depth on NYU-v2. The model used for this comparison is the same as used for COCO panoptic segmentation in Table 1.

METHOD	NYUv2		COCO
	RMSE $\downarrow$	ABS. REL. $\downarrow$	PQ $\uparrow$
DINOv2-LIN1	0.384	-	$\times$
DINOv2-LIN4	0.333	-	$\times$
DINOv2-DPT	0.293	-	$\times$
PAINTER	<b>0.288</b>	0.080	43.3
OURS	0.315	<b>0.078</b>	<b>54.5</b>

validation set consisting of 654 images. They are labeled for metric depth from 0.001 to 10 meters.

### 5.1. Setup and implementation details

Although we work with dense prediction tasks, we use output images of smaller size. This is done for computational reasons. As DINOv2 is trained with patch size of 14, it outputs patch-level embeddings with resolution  $\frac{H}{14} \times \frac{W}{14}$ . We upscale these 8 times, resulting in final output of size  $8\frac{H}{14} \times 8\frac{W}{14}$ . For instance, if the input image is of size  $840 \times 840$ , then the output is of size  $480 \times 480$ . This is similar to the approach used in Pix2Seq-D (Chen et al., 2023).

**Implementation details.** We use DINOv2 (Oquab et al., 2023) as a vision encoder. For the ablation studies we use the 12 layer ViT-Base model. Our main results are reported using the 24 layer ViT-Large model. The shared lightweight decoder consists of 3 transposed convolutional layers (Long et al., 2015) and one convolutional layer. Each of the first three layers upscales the representation  $2\times$ . The input to the decoder comes from concatenating four output layers of the

encoder. When using the 24-layer ViT-Large encoder, we take the output from layers 5, 12, 18 and 24. When using the 12-layer ViT-Base encoder, we take the output from layers 3, 6, 9 and 12. We use AdamW (Loshchilov & Hutter, 2019) optimizer with learning rate of  $5 \times 10^{-4}$ . The learning rate is decayed through a cosine schedule (Loshchilov & Hutter, 2016) after a linear warm up. We do not freeze the weight of the backbone, but use layer decay to suppress the learning rate for the earlier layers.

**Training setup.** We train our models in three stages. This is motivated by two reasons. First, training a ViT-Large backbone with large images is computationally expensive. That is why we first train, over many epochs, with small image sizes and aggressive cropping augmentations. Then we train for a small number of epochs with large image sizes with less or no cropping. The second reason is that the class-agnostic instance segmentation task is much more challenging than semantic segmentation. Note, that the model needs to know the exact location of the center of mass of an instance to predict it correctly. That is why we first train only on the instance segmentation task and then continue with the other tasks in a multi-tasking setup. Additionally, when pretraining for depth, we use a relative depth prediction task with pseudo labels from DepthAnythingV2 (Yang et al., 2024b).

Here are the three stages concretely. Stage 1: Training is only on the class-agnostic instance segmentation task. The input image size is  $280 \times 280$ . Training runs for 400 epochs with effective batch size of 1024. Stage 2: Training is perform on all tasks. For semantic and instance segmentation we use MS-COCO. Depth is optional in this stage. When it is included, it is on the MS-COCO and NYUv2 datasets with pseudo labels from DepthAnythingV2. Training is done for 200 epochs with effective batch size of 512. The input image size is  $336 \times 336$ . Stage 3: This is the final finetuning stage with large images. Training runs for 50 epochs with effective batch size of 16, with images of size  $1008 \times 1008$ . Since the Cityscapes dataset is much smaller we fine-tune on it separately for 400 epochs with images of size  $784 \times 1568$ . The dataset is not included in the first two stages.

**Inference and evaluation.** For the depth prediction task we only need to scale the final output of each pixel. For example, with NYUv2 we have a sigmoid after the last layer and thus the output is in the range  $[0 - 1]$ . We have to multiply the output values by the maximum depth of the dataset (in this case 10). For panoptic segmentation we need to combine the semantic and instance segmentation predictions. Since our model produces a continuous output for each pixel, we have to perform a post-processing step. It includes nearest-neighbor search to attach each pixel to one

Table 3. Panoptic segmentation results on Cityscapes-val dataset.

METHOD	PQ $\uparrow$
<i>Specialized methods:</i>	
ONEFORMER (JAIN ET AL., 2023)	<b>68.5</b>
MASK2FORMER (CHENG ET AL., 2022)	66.6
KMAX-DEEPLAB (YU ET AL., 2022)	68.4
<i>Generalist methods:</i>	
PIX2SEQ-D (CHEN ET AL., 2023)	64.0
OURS	<b>64.2</b>

of a discrete set of possible centroids. Then we perform non-maximal suppression similarly to Painter (Wang et al., 2023). The final step is to combine the class-agnostic instances with the semantic labels using majority voting.

## 5.2. Results

**Panoptic segmentation on COCO.** We report our results on the val2017 split, including a model trained only on panoptic segmentation on COCO, and one trained in a multi-tasking setup with depth. You can see the results in Table 1. The specialized methods we compare to are MaskFormer (Cheng et al., 2021), Mask2Former (Cheng et al., 2022), OneFormer (Jain et al., 2023), kMax-DeepLab (Yu et al., 2022) and Mask-Dino (Li et al., 2023). While still not matching their performance, we significantly shrink the gap between specialized and generalist solutions.

From the generalist approaches LDM-Seg (Van Gansbeke & De Brabandere, 2024) and Pix2Seq-D (Chen et al., 2023) are diffusion based. Painter (Wang et al., 2023) is a multi-tasking model which performs centroid regression, similarly to us. See example predictions on the COCO dataset in Figure 7.

**Depth prediction on NYUv2.** The results we report on NYUv2 are using the exact same model from the COCO panoptic segmentation results. See its performance in Table 2. We do not have depth specific contributions in our work. The main goal of adding the depth task is to verify that our solution is generalist. This is why we use finetuning DINOv2 as a baseline. The performance of our model is on par, while achieving very strong panoptic quality results. DINO’s linear head is most similar to our shared decoder, however DINO achieve better results using a DPT head (Ranftl et al., 2021) as decoder. In our experiments the linear decoder performed better on the panoptic task, thus it is our decoder of choice in all reported results.

**Panoptic segmentation on Cityscapes.** Our approach for Cityscapes (Cordts et al., 2016) is similar to the one used in Pix2Seq-D (Chen et al., 2023). We take a Stage 2 model pretrained only on COCO and finetune for 400 epochs on



## 7. Acknowledgements

This research was partially funded by the dAEdge project (HORIZON-CL4-2022-HUMAN-02-02, Grant Agreement Number: 101120726) and the Ministry of Education and Science of Bulgaria (support for INSAIT, part of the Bulgarian National Roadmap for Research Infrastructure). It was also supported with computational resources provided by Google Cloud Platform (GCP).

## References

- Bellman, R. *Adaptive Control Processes: A Guided Tour*. Princeton Legacy Library. Princeton University Press, 1961. ISBN 9780691079011. URL <https://books.google.bg/books?id=POAmAAAAMAAJ>.
- Bellman, R. and Corporation, R. *Dynamic Programming*. Rand Corporation Research Study. Princeton University Press, 1959. URL [https://books.google.bg/books?id=Pfgtj\\_klGsoC](https://books.google.bg/books?id=Pfgtj_klGsoC).
- Birkl, R., Wofk, D., and Müller, M. Midas v3. 1—a model zoo for robust monocular relative depth estimation. *arXiv preprint arXiv:2307.14460*, 2023.
- Carion, N., Massa, F., Synnaeve, G., Usunier, N., Kirillov, A., and Zagoruyko, S. End-to-end object detection with transformers. In *European conference on computer vision*, pp. 213–229. Springer, 2020.
- Chen, T., Li, L., Saxena, S., Hinton, G., and Fleet, D. J. A generalist framework for panoptic segmentation of images and videos. In *Proceedings of the IEEE/CVF International Conference on Computer Vision*, pp. 909–919, 2023.
- Cheng, B., Collins, M. D., Zhu, Y., Liu, T., Huang, T. S., Adam, H., and Chen, L.-C. Panoptic-deeplab: A simple, strong, and fast baseline for bottom-up panoptic segmentation. In *Proceedings of the IEEE/CVF conference on computer vision and pattern recognition*, pp. 12475–12485, 2020.
- Cheng, B., Schwing, A., and Kirillov, A. Per-pixel classification is not all you need for semantic segmentation. *Advances in neural information processing systems*, 34: 17864–17875, 2021.
- Cheng, B., Misra, I., Schwing, A. G., Kirillov, A., and Girdhar, R. Masked-attention mask transformer for universal image segmentation. In *Proceedings of the IEEE/CVF conference on computer vision and pattern recognition*, pp. 1290–1299, 2022.
- Chiu, M. T., Xu, X., Wei, Y., Huang, Z., Schwing, A. G., Brunner, R., Khachatrian, H., Karapetyan, H., Dozier, I., Rose, G., et al. Agriculture-vision: A large aerial image database for agricultural pattern analysis. In *Proceedings of the IEEE/CVF Conference on Computer Vision and Pattern Recognition*, pp. 2828–2838, 2020.
- Corcuds, M., Omran, M., Ramos, S., Rehfeld, T., Enzweiler, M., Benenson, R., Franke, U., Roth, S., and Schiele, B. The cityscapes dataset for semantic urban scene understanding. In *Proceedings of the IEEE conference on computer vision and pattern recognition*, pp. 3213–3223, 2016.
- Crum, W. R., Camara, O., and Hill, D. L. Generalized overlap measures for evaluation and validation in medical image analysis. *IEEE transactions on medical imaging*, 25(11):1451–1461, 2006.
- Darbyshire, M., Sklar, E., and Parsons, S. Hierarchical mask2former: Panoptic segmentation of crops, weeds and leaves. *arXiv preprint arXiv:2310.06582*, 2023.
- Dosovitskiy, A., Beyer, L., Kolesnikov, A., Weissenborn, D., Zhai, X., Unterthiner, T., Dehghani, M., Minderer, M., Heigold, G., Gelly, S., Uszkoreit, J., and Houshy, N. An image is worth 16x16 words: Transformers for image recognition at scale. In *International Conference on Learning Representations*, 2021. URL <https://openreview.net/forum?id=YicbFdNTTy>.
- Eigen, D., Puhrsch, C., and Fergus, R. Depth map prediction from a single image using a multi-scale deep network. *Advances in neural information processing systems*, 27, 2014.
- He, K., Gkioxari, G., Dollár, P., and Girshick, R. Mask r-cnn. In *Proceedings of the IEEE international conference on computer vision*, pp. 2961–2969, 2017.
- Jain, J., Li, J., Chiu, M. T., Hassani, A., Orlov, N., and Shi, H. Oneformer: One transformer to rule universal image segmentation. In *Proceedings of the IEEE/CVF Conference on Computer Vision and Pattern Recognition*, pp. 2989–2998, 2023.
- Jernigan, M. and McLean, G. Lateral inhibition and image processing. In *Nonlinear Vision: Determination of Neural Receptive Fields, Function, and Networks*, pp. 451–462. CRC press, 2018.
- Kendall, A., Gal, Y., and Cipolla, R. Multi-task learning using uncertainty to weigh losses for scene geometry and semantics. In *Proceedings of the IEEE conference on computer vision and pattern recognition*, pp. 7482–7491, 2018.
- Kirillov, A., He, K., Girshick, R., Rother, C., and Dollár, P. Panoptic segmentation. In *Proceedings of the IEEE/CVF conference on computer vision and pattern recognition*, pp. 9404–9413, 2019.

- Kuhn, H. W. The hungarian method for the assignment problem. *Naval research logistics quarterly*, 2(1-2):83–97, 1955.
- Li, F., Zhang, H., Xu, H., Liu, S., Zhang, L., Ni, L. M., and Shum, H.-Y. Mask dino: Towards a unified transformer-based framework for object detection and segmentation. In *Proceedings of the IEEE/CVF Conference on Computer Vision and Pattern Recognition*, pp. 3041–3050, 2023.
- Lin, T.-Y., Maire, M., Belongie, S., Hays, J., Perona, P., Ramanan, D., Dollár, P., and Zitnick, C. L. Microsoft coco: Common objects in context. In *ECCV*, 2014.
- Livingstone, M. S. *Vision and art (updated and expanded edition)*. Abrams, 2022.
- Long, J., Shelhamer, E., and Darrell, T. Fully convolutional networks for semantic segmentation. In *Proceedings of the IEEE conference on computer vision and pattern recognition*, pp. 3431–3440, 2015.
- Loshchilov, I. and Hutter, F. Sgdr: Stochastic gradient descent with warm restarts. *arXiv preprint arXiv:1608.03983*, 2016.
- Loshchilov, I. and Hutter, F. Decoupled weight decay regularization. In *International Conference on Learning Representations*, 2019. URL <https://openreview.net/forum?id=Bkg6RiCqY7>.
- Lu, J., Clark, C., Zellers, R., Mottaghi, R., and Kembhavi, A. Unified-io: A unified model for vision, language, and multi-modal tasks. In *The Eleventh International Conference on Learning Representations*, 2022.
- Lu, J., Clark, C., Lee, S., Zhang, Z., Khosla, S., Marten, R., Hoiem, D., and Kembhavi, A. Unified-io 2: Scaling autoregressive multimodal models with vision language audio and action. In *Proceedings of the IEEE/CVF Conference on Computer Vision and Pattern Recognition*, pp. 26439–26455, 2024.
- Menze, B. H., Jakab, A., Bauer, S., Kalpathy-Cramer, J., Farahani, K., Kirby, J., Burren, Y., Porz, N., Slotboom, J., Wiest, R., et al. The multimodal brain tumor image segmentation benchmark (brats). *IEEE transactions on medical imaging*, 34(10):1993–2024, 2014.
- Mildenhall, B., Srinivasan, P. P., Tancik, M., Barron, J. T., Ramamoorthi, R., and Ng, R. Nerf: Representing scenes as neural radiance fields for view synthesis. *Communications of the ACM*, 65(1):99–106, 2021.
- Mohan, R. and Valada, A. Efficientps: Efficient panoptic segmentation. *International Journal of Computer Vision*, 129(5):1551–1579, 2021.
- Oquab, M., Darcet, T., Moutakanni, T., Vo, H., Szafraniec, M., Khalidov, V., Fernandez, P., Haziza, D., Massa, F., El-Nouby, A., et al. Dinov2: Learning robust visual features without supervision. *arXiv preprint arXiv:2304.07193*, 2023.
- Ranftl, R., Bochkovskiy, A., and Koltun, V. Vision transformers for dense prediction. In *Proceedings of the IEEE/CVF international conference on computer vision*, pp. 12179–12188, 2021.
- Rudin, L. I., Osher, S., and Fatemi, E. Nonlinear total variation based noise removal algorithms. *Physica D: nonlinear phenomena*, 60(1-4):259–268, 1992.
- Šarić, J., Oršić, M., and Šegvić, S. Panoptic swiftnet: Pyramidal fusion for real-time panoptic segmentation. *Remote sensing*, 15(8):1968, 2023.
- Silberman, N., Hoiem, D., Kohli, P., and Fergus, R. Indoor segmentation and support inference from rgb-d images. In *Computer Vision—ECCV 2012: 12th European Conference on Computer Vision, Florence, Italy, October 7-13, 2012, Proceedings, Part V 12*, pp. 746–760. Springer, 2012.
- Sudre, C. H., Li, W., Vercauteren, T., Ourselin, S., and Jorge Cardoso, M. Generalised dice overlap as a deep learning loss function for highly unbalanced segmentations. In *Deep Learning in Medical Image Analysis and Multimodal Learning for Clinical Decision Support: Third International Workshop, DLMIA 2017, and 7th International Workshop, ML-CDS 2017, Held in Conjunction with MICCAI 2017, Québec City, QC, Canada, September 14, Proceedings 3*, pp. 240–248. Springer, 2017.
- Van Gansbeke, W. and De Brabandere, B. A simple latent diffusion approach for panoptic segmentation and mask inpainting. *arXiv preprint arXiv:2401.10227*, 2024.
- Vasconcelos, N. and Cai, Z. Cascade r-cnn delving into high quality object detection. In *2018 IEEE/CVF Conference on Computer Vision and Pattern Recognition*, 2017.
- Vaswani, A., Shazeer, N., Parmar, N., Uszkoreit, J., Jones, L., Gomez, A. N., Kaiser, Ł., and Polosukhin, I. Attention is all you need. *Advances in neural information processing systems*, 30, 2017.
- Wang, X., Wang, W., Cao, Y., Shen, C., and Huang, T. Images speak in images: A generalist painter for in-context visual learning. In *Proceedings of the IEEE/CVF Conference on Computer Vision and Pattern Recognition*, pp. 6830–6839, 2023.

- Yang, L., Kang, B., Huang, Z., Xu, X., Feng, J., and Zhao, H. Depth anything: Unleashing the power of large-scale unlabeled data. In *Proceedings of the IEEE/CVF Conference on Computer Vision and Pattern Recognition*, pp. 10371–10381, 2024a.
- Yang, L., Kang, B., Huang, Z., Zhao, Z., Xu, X., Feng, J., and Zhao, H. Depth anything v2. *arXiv preprint arXiv:2406.09414*, 2024b.
- Yu, Q., Wang, H., Qiao, S., Collins, M., Zhu, Y., Adam, H., Yuille, A., and Chen, L.-C. kmax-deeplab: k-means mask transformer. *arXiv preprint arXiv:2207.04044*, 2022.
- Zhang, D., Song, Y., Liu, D., Jia, H., Liu, S., Xia, Y., Huang, H., and Cai, W. Panoptic segmentation with an end-to-end cell r-cnn for pathology image analysis. In *Medical Image Computing and Computer Assisted Intervention—MICCAI 2018: 21st International Conference, Granada, Spain, September 16-20, 2018, Proceedings, Part II 11*, pp. 237–244. Springer, 2018.
- Zhang, P., Liu, W., Wang, H., Lei, Y., and Lu, H. Deep gated attention networks for large-scale street-level scene segmentation. *Pattern Recognition*, 88:702–714, 2019.
- Zhen, M., Wang, J., Zhou, L., Fang, T., and Quan, L. Learning fully dense neural networks for image semantic segmentation. In *Proceedings of the AAAI conference on artificial intelligence*, volume 33, pp. 9283–9290, 2019.
- Zhu, Y., Sapra, K., Reda, F. A., Shih, K. J., Newsam, S., Tao, A., and Catanzaro, B. Improving semantic segmentation via video propagation and label relaxation. In *Proceedings of the IEEE/CVF conference on computer vision and pattern recognition*, pp. 8856–8865, 2019.

## A. Details for training depth models

For the depth prediction tasks we follow the approach used in DepthAnything v2 (Yang et al., 2024b). During pretraining in Stage 2 we train on relative depth using pseudo labels coming from DepthAnythingv2 (Yang et al., 2024b). During finetuning in Stage 3 we train on metric depth using NYUv2 (Silberman et al., 2012) labels. This allows us to use more diverse data while pretraining and only learn metric depth for the indoor scenes of NYU at the very end. The two tasks require different approach for the loss. The loss functions we used are explained in the rest of this section.

**Relative depth with pseudo labels.** While pretraining we use images from both COCO (Lin et al., 2014) and NYUv2 (Silberman et al., 2012). Combined they contain a diverse set of outdoor and indoor scenes with varying scales. This is why we follow the approach from MiDaS (Birkel et al., 2023) and DepthAnything (Yang et al., 2024a;b), where we work in disparity space. Since both works do not share training code we had to reproduce the loss ourselves. It will be shared with the rest of our source code. In disparity space we work with  $d$  which is  $1/\text{depth}$  normalized to be between 0 and 1. Then we use affine-invariant loss to compensate for the unknown scale of each image,

$$\mathcal{L} = \frac{1}{HW} \sum_{i=1}^{HW} \rho(d_i^* - d_i), \quad (6)$$

where  $d_i^*$  and  $d_i$  are the ground truth and predictions in the disparity space.  $\rho$  is the affine-invariant loss, i.e.  $\rho(d_i^*, d_i) = |\hat{d}_i^* - \hat{d}_i|$ .  $\hat{d}_i$  is the scaled and shifted version of  $d_i$ , i.e.

$$\hat{d}_i = \frac{d_i - t(d)}{s(d)}, \quad (7)$$

where  $t(d)$  and  $s(d)$  are used to align the scale and median of the predictions and targets.

$$t(d) = \text{median}(d), \quad s(d) = \frac{1}{HW} \sum_{i=1}^{HW} |d_i - t(d)|. \quad (8)$$

**Metric depth.** Finally, in Stage 3, we finetune the model on the metric labels of NYUv2. We use a scale-invariant log loss similar to (Eigen et al., 2014).

$$\mathcal{L} = \frac{1}{n} \sum_i d_i^2 - \lambda \left( \frac{1}{n} \sum_i d_i \right)^2, \quad (9)$$

where  $d_i = \log y_i - \log y_i^*$  is the log difference between the metric prediction and target. We used a value of 0.5 for  $\lambda$ .

## B. Additional losses

As mentioned in the paper we use two additional losses to help us train a better model.

**Total variation loss** With edge distance sampling we don't include the inner parts of objects when computing the loss. Also, the output of our model is continuous prediction for each pixel. However, the desired output for both the semantic and class-agnostic instance segmentation tasks is discrete masks. This is why we use total variation loss (Rudin et al., 1992) as a form of regularization. This loss is penalizing the model when the output of a given pixel is different from its neighbors. This is not desirable only for pixel that are at the border between different objects. The total number of such pixels is negligible. The definition of the total variation loss for a pixel  $i, j$  is as follows

$$l_{i,j}^{tv} = \|\mathbf{y}_{i,j} - \mathbf{y}_{i-1,j}\| + \|\mathbf{y}_{i,j} - \mathbf{y}_{i,j-1}\| \quad (10)$$

Here  $y_{i,j}$  is the output of the model for pixel  $i, j$ . The norm used depends on the main loss. If the main loss is  $L_1$  or  $L_2$ , the norm here is the same. For the instance segmentation task with positional embeddings the norm is the euclidean distance between the two embeddings.

When the main loss is cross entropy as in the semantic segmentation task, the total variation loss is defined as

$$\mathcal{L}_{tv} = \sum_{i=1}^{H-1} \sum_{j=1}^{W-1} \frac{1}{2} (\mathcal{H}(P_{i,j}, P_{i+1,j}) + \mathcal{H}(P_{i,j}, P_{i,j+1})) \quad (11)$$

where  $\mathcal{H}(a, b) = -a \log(b)$  and  $P_{i,j}$  is the probability distribution defined by the logits of the output for pixel  $(i, j)$ .

**DICE Loss** With edge distance sampling we ignore most of the unlabeled pixels when computing the loss, except in the globally applied total variation loss. This is good, because we don't know what is the correct label there. However, we know that whatever this label is it should not be the same as one of the already labeled instances. To enforce this we use a generalized DICE loss (Sudre et al., 2017; Crum et al., 2006). This loss is an approximation of the mean intersection over union.

$$\mathcal{L}_{dice} = 1 - 2 \frac{\sum_l w_l \sum_{i,j} r_{l,(i,j)} p_{l,(i,j)}}{\sum_l w_l \sum_{i,j} (r_{l,(i,j)} + p_{l,(i,j)})} \quad (12)$$

Here,  $l$  is iterating over all labeled instances, while  $i, j$  are iterating over all pixels.  $w_l$  is the weight for each labeled instance. In our case  $w_l = 1/\text{Area}_l$ .  $r_{l,(i,j)}$  is the participation of pixel  $i, j$  to the instance  $l$  according to the ground truth, while  $p_{l,(i,j)}$  is the prediction of the fuzzy participation of pixel  $i, j$  to instance  $l$ .

$$r_{l,(i,j)} = \begin{cases} 1, & \text{if pixel } i, j \text{ belong to instance } l \\ 0, & \text{otherwise} \end{cases} \quad (13)$$

For the instance segmentation task with positional embeddings  $p_{l,(i,j)}$  is a score between 0 and 1, showing how likely the prediction for pixel  $i, j$  belong to instance  $l$ . Remember that  $\bar{y}_{i,j} \in \mathbb{R}^{4L}$ . The first  $2L$  dimensions are the positional embedding of the  $x$  coordinate of the center of mass of the instance to which the pixel belongs. While the last  $2L$  dimensions are the positional embedding of the  $y$  coordinate. Let  $d_{i,j}^x$  and  $d_{i,j}^y$  be the euclidean distance between the ground truth and prediction for the embeddings of the  $x$  and  $y$  coordinates, respectively. Then,

$$p_{l,(i,j)} = e^{-(d_{i,j}^x)^2} e^{-(d_{i,j}^y)^2} \quad (14)$$

### C. Alternative encodings for instance segmentation

Here we explain the alternatives we used to positional embeddings when regressing to the centroid for encoding the instances. There are two options, regression to the  $u, v$  coordinates of the centroid and classification with cross entropy loss.

**RGB encodings for centroid regression.** Painter (Wang et al., 2023) used RGB encoding instead of directly predicting the coordinates of the centroid. He have a similar approach in our ablation study. We can directly regress to the  $u$  and  $v$  coordinates of the centroid, but then it is not clear how to encode the void pixels. Instead we use a 3-dimensional RGB encoding, where the red channel was equal the  $u$  coordinate of the centroid normalized to be in the region  $[0, 1]$ , the green channel was similarly equal to the  $v$  coordinate, and the blue channel was 1 only when the pixel was part of an instance. The encoding for the *void* pixels is pure black  $(0, 0, 0)$ . This is the method referred to as **Direct centroid regression** in Table 4.

**Cross entropy** We divide the image in  $80 \times 80$  grid cells and consider all centroids within a given cell to be the same. This allows us to solve the class-agnostic instance segmentation as a classification problem with 6400 categories. Performing this was too computationally expensive as we need 6400 logits for each pixel. Instead we classified independently the  $u$  and  $v$  coordinates of the center of mass into 80 classes. This is a much more computationally efficient solution. Performance is not

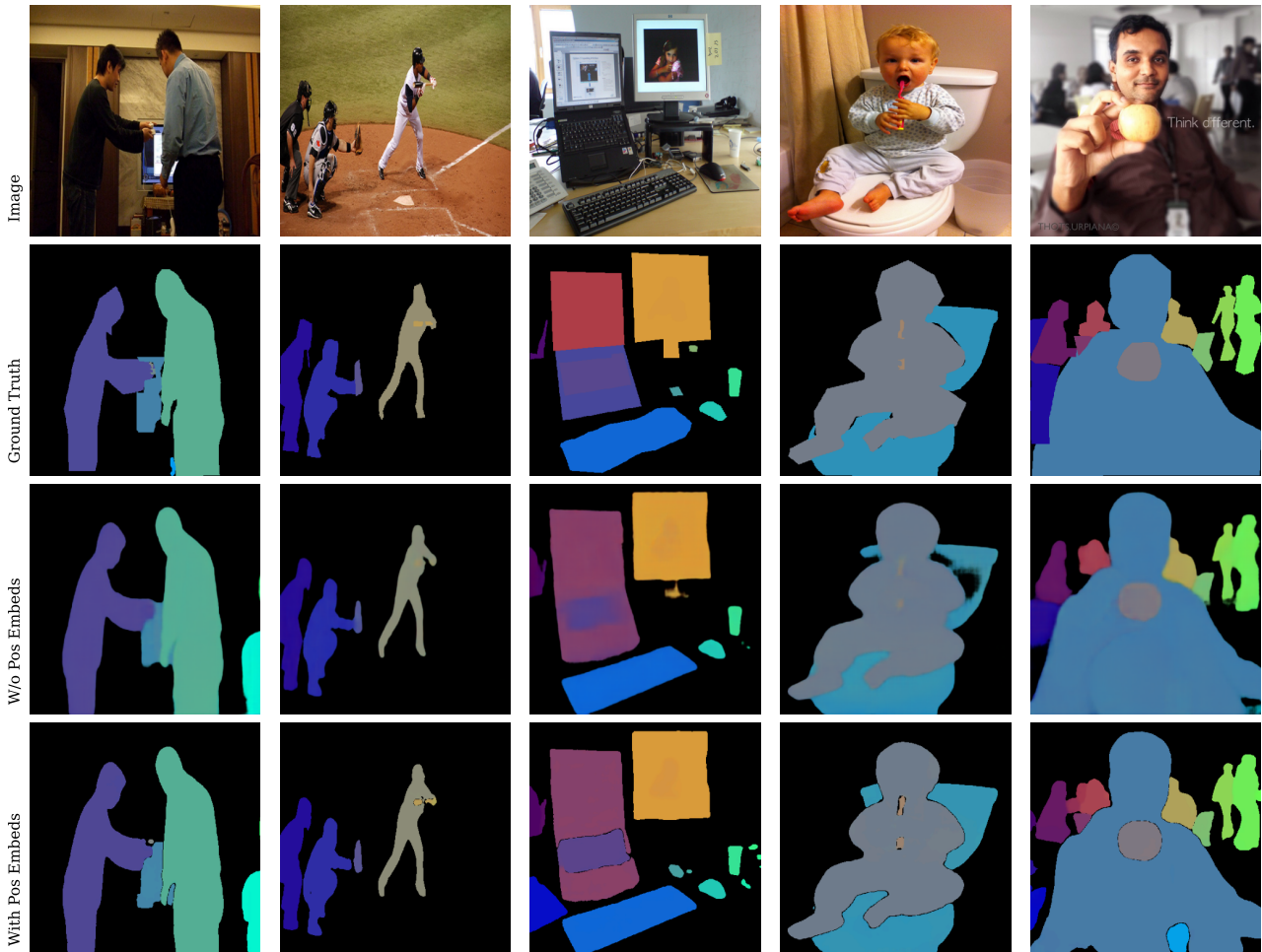


Figure 8. Comparing instance segmentation predictions with and without positional embeddings. It is clear how the boundaries between instances are much less blurry with positional embeddings. When training without positional embeddings the model learn the boundaries with void the best, but struggle with boundaries between objects, especially if the centers of mass are close. Both of these models are trained with DinoV2-Base backbone with image size  $420 \times 420$ .

good, because the cross entropy loss has no concept of distance. Thus small mistakes when the center of mass is challenging to compute, or when the ground truth mask is not precise, lead to problems with training.

### D. Qualitative examples

Here we saw visual demonstration of the effect of positional embedding based loss for instance segmentation. Figure 8 shows examples predictions from the models used for the ablation studies. You can clearly see that adding PE based encoding leads to much better defined boundaries.